International Journal of Environmental Science and Technology
https://doi.org/10.1007/s13762-024-05924-x

ORIGINAL PAPER

The effect of carbon coating on the arsenite sorption by magnetic carbon nanocomposites

A. A. Burbano[1] · V. L. Lassalle[1] · M. F. Horst[1] · G. Gascó[2] · A. Méndez[3]

Received: 8 September 2023 / Revised: 29 May 2024 / Accepted: 28 July 2024

Abstract

Arsenic pollution has emerged through anthropogenic activities and natural mineral leaching processes. This study aims to advance the use of magnetic carbon nanocomposites (MCNs) in the sorption of arsenic, studying the influence of feedstock and the presence of carbon coating on magnetic nanoparticles. Previous works have shown that post-pyrolysis treatment improves the stability of MCNs by reducing iron leaching due to the formation of a carbon coating that encapsulates the iron oxide nanoparticles. However, this carbon coating could influence the adsorption properties of MCNs. This investigation deals with arsenic adsorption by four MCNs prepared by co-precipitation of magnetite (Fe_3O_4) nanoparticle into four carbonaceous matrixes, followed by a post-pyrolysis treatment. The pristine carbonaceous matrixes used in the present work were commercial activated carbon (CAC), charcoal (CC), hydrochar from the orange residue (HC_{OR}), and biochar from sunflower husk (BC_{SFH}). Pristine carbonaceous materials and MCNs without post-pyrolyzed were also used as arsenic sorbents in water solutions. Additionally, kinetic studies were carried out to explore the sorption properties of different MCNs and pristine materials, concerning the removal efficiencies (expressed as a percentage) and adsorption capacities, determining the equilibrium time. The results demonstrated that the presence of magnetite increases the adsorption of arsenic, being higher in the case of materials obtained by direct co-precipitation than in materials subjected to a post-pyrolysis process. The presence of a carbon layerprotecting the magnetite slightly decreases the adsorption of arsenic.

Keywords Arsenite · Biochar · Hydrochar · Carbon nanocomposite · Magnetic materials

Introduction

Arsenic (As) has been recognised as one of the most toxic elements for humans, fauna, and flora. It has been classified by the World Health Organisation (WHO) as a group 1 human carcinogenic substance. According to WHO, the permissible arsenic level of drinking water has been restricted to 10 mg L^{-1} (Bali and Sidhu 2021; Fatoki and Badmus 2022). A report from WHO (WHO 2017) suggests that millions of people worldwide are exposed to higher concentrations of arsenic in drinking water. India, China, Central Africa, and Latin America are the regions most affected for this reason. In this context, Chile, Mexico, and Argentina are the leading countries with critical arsenic concentrations in water sources for human consumption (Litter et al. 2010). In particular, Argentina has a population exposed to arsenic concentrations above 10 mg L^{-1}, which is around 10% of the total population of the country (Bundschuh et al. 2012). The risk to which the population is subjected, especially those found in rural environments, makes the presence of arsenic in groundwater a topic of interest for immediate resolution for the government due to the impact on the health of a large part of the population. Arsenic contamination in groundwater can occur naturally through biogeochemical or anthropogenic activities such as acid mine drainage, petroleum refining, ceramic manufacturing industries, and coal combustion (Rathi and Kumar 2021; Viraraghavan et al.

Editorial responsibility: S.Mirkia.

✉ A. Méndez
anamaria.mendez@upm.es

[1] Departamento de Química, INQUISUR, Universidad Nacional del Sur (UNS)-CONICET, Av. Alem 1253, 8000 Bahía Blanca, Argentina

[2] Departmento de Producción Agraria, Universidad Politécnica de Madrid, Ciudad Universitaria, 28040 Madrid, Spain

[3] Departamento Ingeniería Geológica y Minera. E.T.S.I. Minas y Energía, Universidad Politécnica de Madrid, Calle Ríos Rosas 21, 28003 Madrid., Spain

Published online: 05 August 2024

1999). Natural sources such as weathering, erosion of rocks/soils, and volcanic emissions also contribute to arsenic in an aqueous system. Various studies have documented the health effects of drinking water with high levels of arsenic, which could cause severe damage, including skin lesions (hyperpigmentation, hyperkeratosis) and different kinds of cancer (kidney, lung, bladder, skin).

Arsenic is used in various applications, such as a preservative for pressure-treating lumber, as a strengthening agent in lead-storage batteries, in pesticides and insecticides, as an antifriction additive for bearings, and as wheel weights for tyres. Another increasingly important use of arsenic is to manufacture gallium-arsenide semiconductors for solar cells and telecommunications. The last list of critical raw materials from the European Commission has included arsenic as critical material (European Commission 2023), increasing the interest in recovery of arsenic from alternative sources.

Several technologies have emerged to remove arsenic compounds, including coagulation and flocculation for chemical precipitation, oxidation, membrane processes, ion exchange, electrolysis and adsorption (Ahmaruzzaman 2022; Pezeshki et al. 2023; Kabir and Chowdhury 2017; Rathi and Kumar 2021; Saravannan et al. 2023). Most of them need a pre-treatment step, are expensive or generated a large amount of waste (Saravannan et al. 2023). For example, the use of membrane processes, especially nanofiltration or reverse osmosis, is one of the most effective methods for arsenic removal in the absence of chemicals. However, the main disadvantages of this technology are the high investment cost, the formation of membrane sediments, and the high energy consumption (Alka et al. 2021). The precipitation process is simple. Chemicals are added to destabilize and convert the dissolved arsenic compounds into insoluble precipitates. The process may be used in conjunction with other techniques and large amounts of toxic sludges are produced. Other technologies, such as ion exchange, exhibit excellent performance on the removal of As (V) but it is difficult to play a role in As (III), being necessary pre-oxidation treatments (Fang et al. 2021). Inorganic arsenite, As (III), and arsenate, As (V), are the predominant arsenic species in water. Among them, As (III) is more toxic and mobile than As (V). Furthermore, As (III) is more difficult to remove from water than As (V) because, at $pH < 9$, it exists as H_3AsO_3. Negatively charged As (III) species, including $H_2AsSO_3^-$, $HAsO_3^{2-}$, and AsO_3^{3-}, are found at a pH higher than 9.2. Consequently, the removal of As (III) in water by adsorption or ion exchange processes is less effective than for As (V), which can exist in the form of different ions in a wide range of pHs (Alkurdi et al. 2021). Oxidation techniques are also used to convert As (III) into As (V) before it is removed by flocculation technologies. The process uses some oxidants such as ferric ions, H_2O_2 or persulfate, and different flocculant compounds (Song et al. 2024). Other advanced technologies such as electrocoagulation lead to higher arsenic removal but are expensive. Kabir and Chowdhury (2017) concluded that future research is needed in simple and low-cost technologies to remove arsenic from water. Adsorption stands out due to its ease of operation, high efficiency, selectivity, versatility, low cost, sludge-free, and environmental friendliness (Lata and Samadder 2016; Uddin and Jeong 2020). Moreover, using nanomaterials as adsorbents in arsenic removal has shown interesting results (Habuda-Stanić and Nujić 2015). Specifically, studies have shown in the last decade that iron oxide nanoparticles are excellent adsorbents for arsenic removal due to their enhanced surface-to-volume ratio, high affinity towards arsenic, low energy consumption, reversibility, and high selectivity (Liu et al. 2015).

Nevertheless, the iron oxide nanoparticles exhibit some drawbacks, such as the aggregation trend resulting from their high surface area, magnetic dipole interactions between particles, and the lack of stability leading to iron leaching (Hao et al. 2018). Consequently, immobilizing iron oxide nanoparticles to avoid the abovementioned limitations mentioned is challenging in nanotechnological applications. Activated carbons are unique carrier materials due to their excellent ability to support nanoparticles, stability, high surface area, and developed porous structure (Shahrashoub and Bakhtiari 2021; Xu et al. 2020). However, commercial activated carbons are expensive because of feedstock manufacturing characteristics and activation processes. These disadvantages have led to the exhaustive finding of economically low-cost alternatives such as carbonaceous materials (biochars and hydrochars) prepared by thermochemical treatments of biomass wastes (Low and Yee 2021; Qin et al. 2022; Sri Shalini et al. 2021; Yihunu et al. 2019). The final physicochemical properties of carbon materials are considerably dependent on initial feedstock properties, heating rate, treatment temperature, reaction pressure, reaction residence time, reaction vessel dimensions, and, in some cases, activating agents that would promote the porosity development during thermal treatment (Colomba et al. 2022; Leng et al. 2021). These carbon materials have been implemented as sorbents in water, as amendments in polluted soil remediation, as supercapacitors or catalysts (Horst et al. 2016; Zhou et al. 2021; Méndez et al. 2022; Kang et al. 2022; Hsiao et al. 2023). However, its recovery from the medium demands tedious and, in some cases, expensive steps that can be solved by introducing an innocuous magnetic component to the carbon material, such as magnetite nanoparticles, to easily separate it by employing an external magnetic field (Qu et al. 2022; Truong et al. 2022).

The stability of iron oxide on the surface of the carbonaceous material greatly depends on the preparation process. At low pHs, iron oxide can be removed from the carbonaceous surface (Burbano et al. 2022). Previous works

performed by our research group (Burbano et al. 2022) have shown that post-pyrolysis treatment reduces iron leaching from MCNs due to the formation of a carbon coating that encapsulates the iron oxide nanoparticles. However, this carbon coating could influence their adsorption properties. In this order of ideas, this investigation aims to advance the use of MCNs as sorbents of arsenic in aqueous samples. The goal of this research is to compare the use of different MCNs and study the influence of feedstock and the presence of carbon coatings on magnetic nanoparticles. For this, four MCNs were obtained by in-situ magnetite (Fe_3O_4) nanoparticle co-precipitation into four carbonaceous matrixes. Then, the four previously obtained MCNs were subjected to post-pyrolysis treatment to coat the magnetic core. The pristine carbonaceous matrix used in the present work was a commercial activated carbon (CAC), charcoal (CC), hydrochar from the orange residue (HC_{OR}), and biochar from sunflower husk (BC_{SFH}). Kinetic studies of arsenite adsorption by different sorbents (MCNs, post-pyrolyzed MCNs and pristine carbonaceous materials) were performed by adjusting pH, temperature, contact time, initial concentration, and sorbent dose.

Materials and methods

Materials

Sodium arsenite was purchased from PanReac Química SA (Spain). Iron (II) sulfate heptahydrate ($FeSO_4{\cdot}7H_2O$, M = 278.02 g mol^{-1} (Barcelona-Spain) was from Labkem. Iron (III) chloride 6-hydrate ($FeCl_3{\cdot}6H_2O$, M = 270.32 g mol^{-1}) was purchased from PanReac AppliChem (Spain). Sodium hydroxide (NaOH, M = 40 g mol^{-1}) was supplied by Merck (Darmstadt-Germany). Commercial activated carbon (CAC) and charcoal (CC) were supplied by PanReac Química SA (Spain) and Ibecosol (Spain), respectively.

Preparation of MCNs and post-pyrolyzed MCNs

Four carbonaceous materials: a commercial activated carbon (CAC), charcoal (CC), hydrochar from the orange residue (HC_{OR}), and biochar from sunflower husk (BC_{SFH}), have been used for the preparation of MCNs and post-pyrolyzed MCNs. The co-precipitation of magnetite nanoparticles was carried out using 35 g Fe^{3+} and 18 g Fe^{2+} (2:1 molar ratio) as iron precursors and an excess of NH_4^+ to promote the formation of magnetite nanoparticles. Later, the four post-pyrolyzed MCNs were prepared through a pyrolysis treatment to cover the magnetic core, as previously widely described by Burbano et al. (2022). Table 1 summarises the preparation conditions and feedstock of 16 materials used in this research.

Characterization of MCNs and post-pyrolyzed MCNs

A wide characterization of MCNs and post-pyrolysis MCNs materials has been performed previously (Burbano et al. 2022; 2023).

Elemental analysis

For these determinations a LECO CHNS 932 analyzer by air dry combustion was used. H/C and O/C ratios were calculated.

Table 1 Experimental conditions used in the preparation of carbon-based materials

Name	Description	Residence time (h)	Temperature (°C)
CAC	Commercial activated carbon	–	–
CC	Commercial charcoal	–	–
HC_{OR}	Hydrochar from orange residue	6	240
BC_{SFH}	Biochar from sunflower husk	2.5	700
MAC	Magnetic activated carbon prepared by co-precipitation of magnetite on CAC	–	25
MCC	Magnetic charcoal prepared by co-precipitation of magnetite on CC	–	25
MHC_{OR}	Magnetic hydrochar from orange residue prepared by co-precipitation of magnetite on HC_{OR}	–	25
MBC_{SFH}	Magnetic hydrochar from sunflower husk prepared by co-precipitation of magnetite on BC_{SFH}	–	25
MACP	Pyrolyzed magnetic activated carbon	2	600
MCCP	Pyrolyzed charcoal	2	600
$MHCP_{OR}$	Pyrolyzed magnetic hydrochar from orange residue	2	600
$MBCP_{SFH}$	Pyrolyzed magnetic biochar from sunflower husk	2	600

Porous properties

The porous properties were determined by N_2 adsorption–desorption using a ASAP 2420 Micromeritics porosimetry system (SCAI-Málaga University). Different methods were employed to obtain the BET surface area, pore volume, and pore sizes, such as BET, BJH, and DFT.

pH

For the determination of pH, aqueous solutions of carbon-based materials were prepared using concentrations of about 4 g L^{-1} in distilled water solution. A Crison micro pH 2000 was used to determine the pH of the solutions.

Zeta potential (ξ)

For ξ measurements, samples containing 5 mg mL^{-1} of material in 0.01 M NaCl were prepared, and the pH was adjusted in the range between 9 and 3 with 0.01 M NaOH or HCl solutions. Measurements were performed in zeta potential analyser (Nano-ZS90X, Malvern, UK).

Electronic microscopy

Transmission electronic microscopy (TEM Jeol 100 CX II) and scanning electronic microscopy (SEM LEO EVO 40 XVP) were used to demonstrate the presence of magnetic nanoparticles, their morphology, and estimate their sizes on the carbonaceous matrixes. The samples were dispersed in distilled water/ethanol, placed on 200 mesh Cu grids, and dried at room temperature.

Batch adsorption experiments

Kinetics adsorption assays were carried out to determine the equilibrium time at which no transformations were observed between adsorption and desorption (plateau formation). Approximately 0.25 g of each material was added to 250 mL of $NaAsO_2$ solution in a flask. The initial $NaAsO_2$ concentration was adjusted at 30 mg L^{-1}. Subsequently, the flasks were transferred to a horizontal shaker at solution pH and room temperature. Aliquots of 1 mL/25 mL were taken every 10, 20, 30, 60, and 120 min. Arsenic was quantified by inductively coupled plasma mass spectrometry (model ICP-MS Elan DRCe (SCIEX Perkin Elmer) from SCAI-Malaga University). The adsorption capacity, $q_{e,}$ (mg g^{-1}) was determined employing the following equation:

$$q_e = \frac{(Ci - Cf)V}{m}$$

where Ci is the initial concentration (mg L^{-1}), Cf is the final concentration (mg L^{-1}), V is the volume of solution (L) and m is the mass used of each material (g).

Adsorption kinetic models

Adsorption kinetic models were adjusted with the experimental kinetics data. Among the existing adsorption kinetic models, including Elovich, Avrami, Crank, Vermeulen, Weber-Morris, Bangham, linear film, mixed surface reaction and diffusion, and multi-exponential models, pseudo first order (PFO) and pseudo-second-order (PSO) classical kinetic models are widely employed (Revellame et al. 2020) These models are used in their linearised forms:

Pseudo-first-order model It was first proposed at the end of the nineteenth century by Langergen. Ho and Mckay (1999) stipulated that this model focusses on the first stage of the adsorption process and assumes physisorption as the rate-limiting step. The linearised form of the PFO model is:

$$\ln\left[q_{e-}q(t)\right] = \ln q_e - k_1 t$$

q is the amount of adsorbed solute (mg g^{-1}), q_e is the amount of adsorbed solute at equilibrium (mg g^{-1}), k_1 is the pseudo-first-order rate constant, and t is the time.

Pseudo-second-order model As indicated by Ho and Mckay (1999), a significant number of studies fitted the PSO. This model considers chemisorption as the rate-limiting mechanism in the adsorption process. The linearised formula of the PSO model is:

$$\frac{t}{q(t)} = \frac{t}{q_e} + \frac{1}{K_2 q_e^2}$$

In which k_2 is the pseudo-second-order kinetic rate constant.

Characterization of post-adsorption materials

To understand possible adsorption mechanisms, the post-adsorption material with the highest arsenite removal efficiency was characterized using FTIR, zeta potential, and DLS techniques.

Results and discussion

Properties of MCNs

Table 2 shows the main characteristics of carbon-based materials (Burbano et al. 2022; 2023). Carbon-based materials, except for HC_{OR} obtained by hydrothermal

Table 2 Main characteristics of carbon-based materials (Burbano et al. 2022; 2023)

Carbon-based material	pH	H/C	O/C	Ash (%)	S_{BET} ($m^2\ g^{-1}$)
CAC	8.03	0.12	0.11	1.00	1139.0
CC	8.31	0.47	0.01	14.94	2.2
HC_{OR}	5.57	0.97	0.34	5.99	7.8
BC_{SFH}	10.48	0.11	0.07	5.49	493.0
MAC	8.50	0.11	0.04	49.83	511.4
MCC	9.50	0.52	0.19	53.54	57.7
MHC_{OR}	9.30	1.06	0.43	56.34	83.5
MBC_{SFH}	8.52	0.17	0.15	50.62	244.1
MACP	8.90	0.01	0.18	52.81	425.0
MCCP	9.73	0.12	0.15	59.09	120.4
$MHCP_{OR}$	10.08	0.12	0.22	73.23	84.3
$MBCP_{SFH}$	8.60	0.08	0.12	52.51	257.2

carbonization, show basic pHs. The highest pH values (> 10) correspond to BC_{SFH} and $MHCP_{OR.}$ The pH of pristine carbonaceous materials (CAC, CC, $HC_{OR,}$ and BC_{SFH}) increases with the co-precipitation of magnetite and the post-pyrolysis treatment. On the other hand, the H/C atomic ratio is an index that reflects the aromaticity of carbonaceous materials. CAC and BCSFH, which were the carbons exposed at higher temperatures, exhibits lower H/C, indicating that their aromaticity was enhanced by increasing temperature. Temperature has been shown to be a crucial factor in the preparation of carbonaceous solids. This parameter is the one that promotes the formation of poly-condensed aromatic rings. The co-precipitation of magnetite increases the H/C values of MCC, MHC_{OR}, and $MBC_{SFH,}$ which indicates the modification of chemical structures decreasing the aromaticity. Only CAC and MAC show similar values (0.11 and 0.12, respectively). The post-pyrolysis treatment decreases the H/C ratios due to the volatilisation of light compounds and condensation reactions. The co-precipitation of magnetite and post-pyrolysis treatment also modifies the O/C ratios. MCNs and post-pyrolyzed MCNs show a higher ash content than pristine carbonaceous materials due to magnetite. Finally, carbon-based materials show a wide range of surface areas. The CAC and BC_{SFH} samples show the highest S_{BET} among the original materials. In this case, the co-precipitation of magnetite decreases the BET area. In the case of CC and HC_{OR} samples, co-precipitation of magnetite and post-pyrolysis slightly increase the BET area (Burbano et al. 2022).

SEM and TEM analysis

Transmission Electron Microscopy (TEM Jeol 100 CX II) and Scanning Electron Microscopy (SEM LEO EVO 40 XVP) were used to evidence the presence of magnetic nanoparticles, morphology and estimate their sizes on the carbonaceous matrixes.

The morphology properties of the materials are shown in SEM micrographs (Fig. 1). Micrographs represent the carbonaceous matrixes, the magnetic carbon nanocomposites, and the post-pyrolyzed magnetic carbon nanocomposites. As can be observed, carbonaceous matrixes have a different morphology in terms of the characteristics of their pores. CAC is characterized by its highly developed and homogeneous porous structure. These commercial materials undergo a thermochemical process optimised to obtain microporous materials with high surface area materials applied in different fields. Similarly, BC_{SFH} has ordered pore distribution and pore channels. On the other hand, CC and HC_{OR} have a poor porous structure. This can be attributed to the thermochemical treatments employed: pyrolysis (without an activating agent) and hydrothermal carbonisation. The formation of pores can be related to high temperatures because this exposure leads to the release of volatile matter, which develops the porosity of the materials. When lignocellulosic biomasses is subjected to a thermochemical decomposition, they undertake different chemical reactions like depolymerisation, fragmentation, and cross-linking, which finally produce carbon materials that exhibit recalcitrance and a dense carbonised structure. The SEM results can be supported using N_2 adsorption–desorption isotherms of the carbonaceous matrixes, the magnetic carbon nanocomposites, and the post-pyrolyzed magnetic carbon nanocomposites that have been reported in previous studies (Burbano et al. 2023). In addition, magnetite nanoparticles appear spherically shaped in magnetic carbon nanocomposites (MAC, MCC, MBC_{SFH} and HCOR) in TEM micrographs (second column). Nevertheless, other types of shape, such as anisotropic ones, correspond to the intermediate synthesis process of magnetite nanoparticles such as goethite. The micrographs on the right side (third column) correspond to the post-pyrolyzed magnetic carbon nanocomposites (MACP, MCCP, $MBCP_{SFH}$, $MHCP_{OR}$). Magnetic nanoparticles are inserted into the carbonaceous matrix. In some cases, such as in micrograph of MACP, the carbonaceous matrix tends to form a coating on the surface of the nanoparticles.

Zeta potential as a function of pH

The media's pH is the main factor influencing the zeta potential (ζ). In addition, other factors affect the zeta potential value, such as the ionic strength, particle size, temperature, and dispersion concentration. Table 3 illustrates the sign and magnitude of the zeta potential for the explored pH values. Each material (the carbonaceous matrix, the magnetic carbon nanocomposites, or the post-pyrolyzed magnetic carbon carbon nanocomposites) behaves differently concerning its

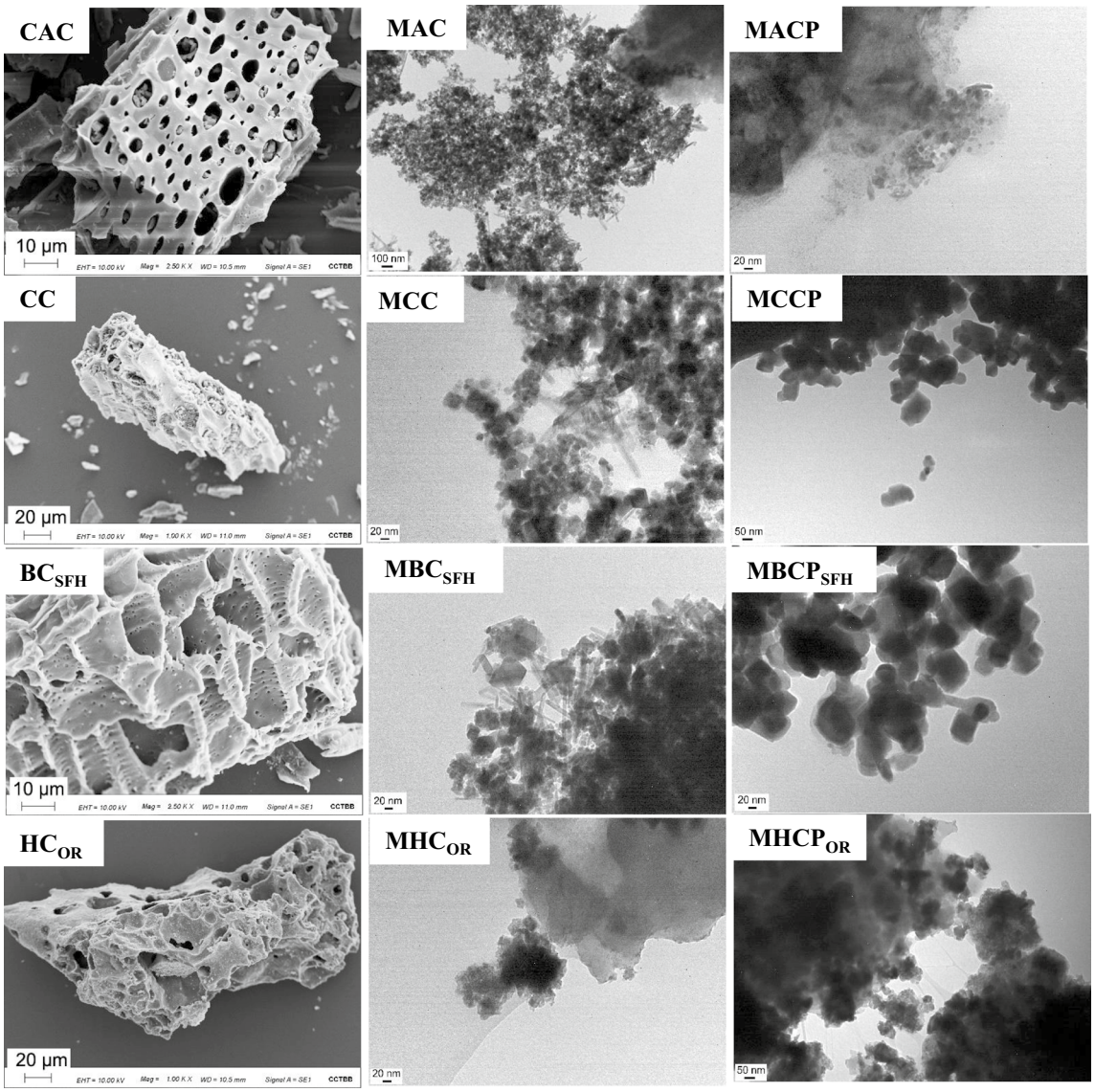

Fig. 1 SEM (first column) and TEM micrographs (second and third columns) of carbonaceous matrixes (CAC, CC, BCSFH and HCOR, magnetic carbon nanocomposites (MAC, MCC, MBCSFH and HCOR) and post-pyrolyzed magnetic carbon nanocomposites (MACP, MCCP, MBCPSFH, MHCPOR)

Table 3 Zeta potential of carbon-based materials at aqueous solution pHs

Material	CAC	CC	BC$_{SFH}$	HC$_{OR}$	MAC	MCC	MBC$_{SFH}$	MHC$_{OR}$	MACP	MCCP	MBCP$_{SFH}$	MHCP$_{OR}$
Isoelectric point	no	no	no	no	5.2	3.6	6.4	3.1	no	3.6	3.6	no
Zpot(mV)	–*	–*	–*	–*					–*			–*

The materials that possess IEP present positive zeta potential above the IEP and negative zeta potential under the IEP

*Negative value zeta potential in all of the studied pH range from 3 to 9

surface charge. The carbonaceous matrix exhibits negative zeta potentials in all the pH range.

In addition, magnetic carbon nanocomposites appear to possess different isoelectric points (IEP) with respect to MAC, MCC, MHC$_{OR}$, and MBC$_{SFH}$. It is worth mentioning that IEP is the pH point at zeta potential, which reaches zero. The IEPs of the above-mentioned materials are 5.2, 3.6, 3.3, and 3.6, respectively. The zeta potential is positive at low

pH and negative at higher pH. On the other hand, the post-pyrolyzed magnetic carbon nanocomposites exhibit different behavior. MACP and MHCP have negative zeta potential from pH 3–9. In contrast, MCCP and $MBCP_{SFH}$ have IEPs, which is 3.6 in both cases. These results indicate that MACP and MHCP exhibit their IEP at very low pH values. These differences in the zeta potential might be due to the presence of different surface functional groups and their ability to protonate and deprotonate at different pHs (Qiu et al. 2022).

The presence of magnetic iron oxide nanoparticles promotes changes in this behavior because of their amphoteric character. It is well known that iron oxides, specifically magnetite/maghemite, exhibit IEP between pH 6.5–7. The coating or even functionalization of these nanoparticles leads to deviation of this pH as IEP, which depends on the interactions between the magnetic and modifier phases. Previous work reported similar results (Horst et al. 2017). For instance, the IEP of nanocomposite prepared by co-precipitation of magnetic nanoparticles on chitosan, of composition magnetic nanoparticles/chitosan 1/0.5, shifted to 5.45. The shift appeared to depend on the composition of nanocomposite since the value of nanocomposite containing magnetic nanoparticles/chitosan 0.5/1 ratio reached IEP at pH 8.3. The higher zeta potential and PZC of chitosan–magnetite particles arise due to a higher proportion of amine groups coming from a more significant amount of chitosan in the nanocomposite (Horst et al. 2016).

Adsorption of arsenite

Figure 2 shows the As removal efficiency (%) at equilibrium time. The highest values of As removal (> 87%) were obtained using MCNs. The presence of magnetite significantly increases the capacity of pristine carbonaceous materials to adsorb arsenite. Additionally, the post-pyrolysis treatment, decreases the removal of arsenite compared to MCNs, specially for MHC_{OR} and $MBCP_{SFH}$. Previous works have shown that MCNs obtained from biochar and hydrochar show the highest stability of the carbon coating compared to commercial charcoal or activated carbon (Burbano et al. 2022). Probably, the coat of magnetic nanoparticles originated during pyrolysis of biochar and hydrochar is more effective than that obtained after the pyrolysis of activated carbon or charcoal, which produces less volatiles. However, in all cases, the pristine carbonaceous materials show less As removal than post-pyrolyzed MCNs.

Figure 3 shows the adsorption kinetics of the non-magnetic carbon-based materials, the MCNs, and the post-pyrolyzed MCNs, demonstrating that all the materials exhibit good adsorption capacities. Non-magnetic carbon-based

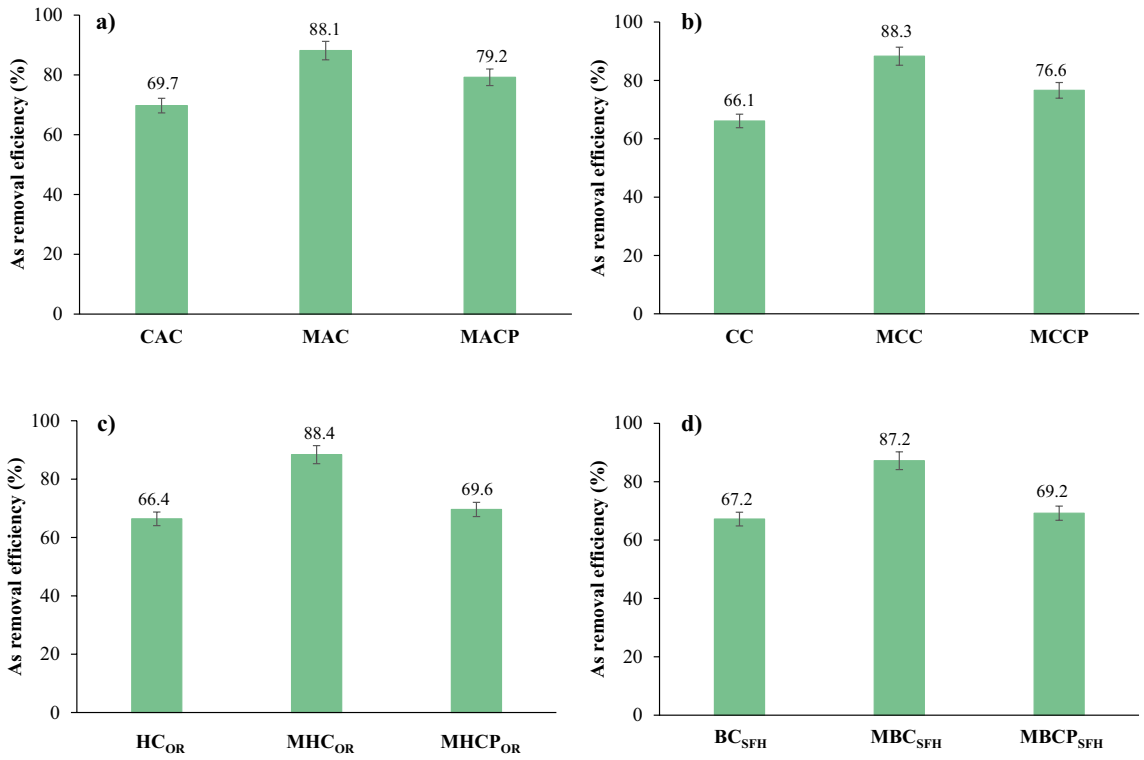

Fig. 2 Arsenic removal efficiency at the equilibrium time of carbon-based materials and magnetic carbon nanocomposites based on: **a** commercial activated carbon (CAC, MAC and MACP), **b** charcoal (CC, MCC and MCCP), **c** hydrochar of orange residue (HCOR, MHCOR and MHCPOR) and **d** biochar of sunflower husk (BCSFH, MBCSFH and MBCPSFH)

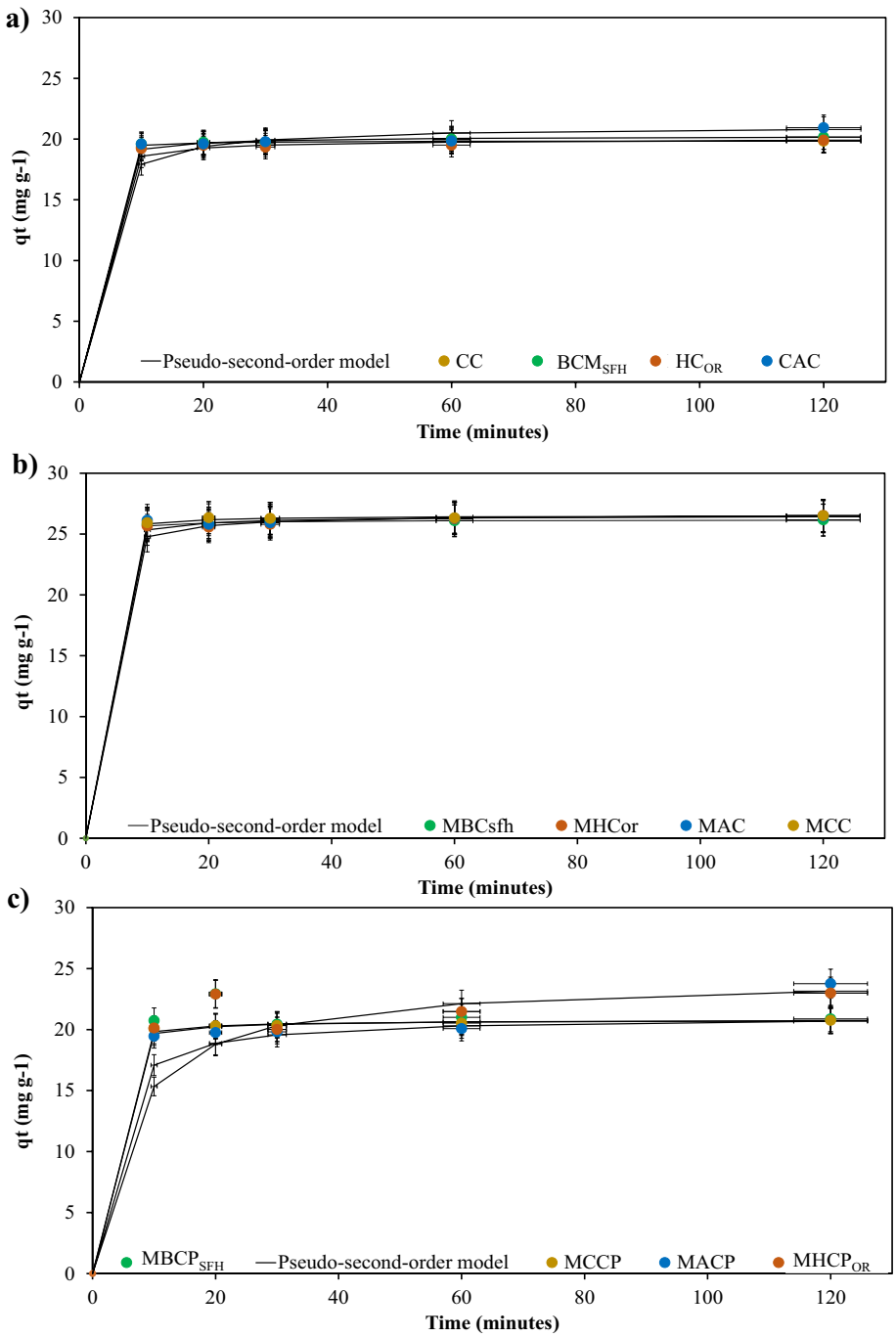

Fig. 3 Adsorption kinetic studies of **a** carbon-based materials, **b** magnetic carbon nanocomposites, and **c** post-pyrolyzed magnetic carbon nanocomposites

materials show As removal efficiencies ranging between 66.11% for CC and 69.73% for CAC. Co-precipitation of magnetite significantly increases As removal efficiency to values from 87.22% for MBC_{SFH} to 88.33% for MCC. The presence of a magnetic phase functions as an adsorption site for As in an aqueous solution by forming an outer sphere and inner layer complexes. These results are comparable with previous study by Wang et al. (2015) where a magnetic biochar was prepared from pinewood and used to remove As. They have found that iron oxide nanoparticles act as adsorption sites to remove As, and that their presence enhances the removal process. In addition, Scheverin et al. (2022) developed iron-based nanocomposites to remove arsenic in real groundwater, obtaining great removal percent efficiencies, and determining that the formation of complexes between arsenic and iron oxide moieties can explain the adsorption mechanisms.

Finally, post-pyrolysis treatment of magnetic nanocomposites slightly reduces the removal efficiency of As. The highest removal efficiency can be assigned to $MCHP_{OR}$ and

$MBCP_{SFH}$. The adsorption is very rapid within 10 min of contact time. Previous research (Burbano et al. 2022) has shown that these materials exhibit a structure where iron oxide nanoparticles remain carbon-coated. This carbon coat can contribute to the reduction of As adsorption in comparison to the magnetic carbon nanocomposites. However, the removal efficiency is higher than for the non-magnetic carbon nanocomposites. The adsorption capacities of As into the solids depend on different factors, including i) physicochemical characteristics of the adsorbent materials, ii) physicochemical properties of the adsorbate, and iii) adsorption conditions (pH, agitation rate, temperature, arsenite initial concentration, and ionic strength). The carbon adsorbent materials exhibit i) oxygen-containing functional groups, which can be associated with acid (carboxyl, lactone, phenol, lactol), and basic groups (ketones, pyrones), ii) iron oxide groups, and iii) carbon ring structures. Each of them could interact with arsenite through different adsorption mechanisms. Another important characteristic of these materials is the BET surface area, which could be responsible for their adsorption performance. In this case, it was demonstrated that the surface area of magnetic carbon nanocomposites decreases, and these adsorbents were those that had better arsenite adsorption. Therefore, the surface characteristics of the materials are not the relevant properties by which arsenic adsorption takes place. So, the main mechanism by which the As could be adsorbed in the materials assayed in this study is by forming complexes between iron oxide nanoparticles and arsenite.

Adsorption kinetic models

The experimental data were fitted to both the PFO and PSO kinetic models. The adsorption capacity, the PFO and PSO constants, and the coefficient of determination (R^2) are observed in Table 4. Any modelling requires validation methods. R^2 is a well-known validation method that can be combined with q_e to choose the suitable model for the dataset. As can be illustrated in Table 4, the R^2 values are higher in PSO than in PFO. For this reason, the results fit better to PSO, which assumes that it is applicable over a long period of adsorption time and that the rate-limiting step is chemisorption. Zama et al. (2017) studied the removal of As (III) using biochars prepared at different temperatures and observed that weak electrostatic and ion exchange forces are involved. Also, Navarathna et al. (2019) have prepared magnetic biochar composites where it was seen that the experimental kinetic results best fitted the pseudo-second order model ($R^2 > 0.99$), which suggested that the chemisorption mechanisms were mainly governing. Arsenite oxygen atoms can act like Lewis bases, forming covalent bonds (inner-sphere) Fe–O–As complexes in the place of some Fe–OH surface sites (Zhang et al. 2010).

Characterization of post-adsorption material

MHC_{OR} was selected to analyze after adsorption from all the adsorbents assayed. Figure 4 shows the post-adsorption materials' FTIR spectra, zeta potential, and hydrodynamic diameter. These characterization techniques can contribute to the analysis of materials after adsorption and offer a more detailed understanding of the main interaction pathways. A wide characterization of magnetic carbon nanocomposites has been performed previously (Burbano et al. 2023). The FTIR spectra of Fig. 4 compared two materials, MHC_{OR} and post-adsorption MHC_{OR}. There are differences in molecular vibrations in both spectra. It can be noticed that in the MHC_{OR} post-adsorption spectrum, O–H stretching

Table 4 Kinetic parameters of arsenite adsorption on carbon-based materials

Carbon-based material	PFO*			PSO**		
	q_e	K_1	R^2	q_e	K_2	R^2
CAC	20.94	0.04	0.84	21.09	0.02	0.99
CC	19.97	0.01	0.18	19.88	0.25	1.00
HC_{OR}	19.92	0.04	0.86	20.00	0.06	0.99
BC_{SFH}	20.18	0.03	0.96	20.24	0.08	1.00
MAC	26.45	0.03	0.91	26.52	0.08	1.00
MCC	26.50	0.05	0.88	26.52	0.14	1.00
MHC_{OR}	26.52	0.05	0.93	26.66	0.04	1.00
MBC_{SFH}	26.17	0.02	0.56	26.17	0.19	1.00
MACP	23.77	0.05	0.83	24.27	0.007	0.99
MCCP	23.00	0.04	0.52	21.09	0.02	0.99
$MHCP_{OR}$	20.77	0.04	0.95	20.83	0.08	1.00
$MBCP_{SFH}$	22.94	0.02	0.11	20.79	0.09	0.99

*PFO, pseudo first order kinetic model

**PSO, pseudo-second-order kinetic models

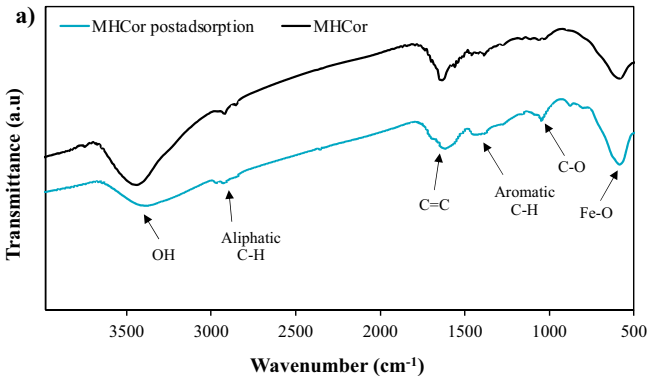

Fig. 4 **a** FTIR spectra and **b** Z potential and hydrodynamic diameter of MHCOH post-adsorption material

b) Sample	pH	Zeta potential	Hydrodynamic diameter (nm)	PDI
MHC_{OR}	5.51	-17.7	1356	0.71
MHC_{OR} post-adsorption	6.12	-12.7	811.3	0.63

vibration (3300–3600 cm^{-1}) shifted to a lower wavenumber (from 3467 to 3400 cm^{-1}), and Fe–O vibration (550 cm^{-1}) still appears, showing that it might form outer complexes. The zeta potential of post-adsorption material acquires a slightly more positive value, and the hydrodynamic diameter is lower than in the initial MHC_{OR}; these results suggest that the arsenite might be attached to the magnetic hydrocarbon material, as was already mentioned. At the pH value of adsorption assays above the zero charge point of the adsorbent material, an electrostatic attraction might be the interactions between arsenite and MHC_{OR}. This contributes to the increase of pH of the adsorbent post-adsorption since the positive functional groups were involved in the interactions, leading to an increment in negative surface charge, as seen in Table 3. Similar results were observed by Wang et al. (2015) by magnetic biochar synthesized by direct pyrolysis of hematite-treated biomass and assayed for As adsorption.

Conclusion

Magnetic carbon nanocomposites exhibit great potential as environmental remediation tools in arsenite adsorption. Even though carbonaceous solids possess high percent removal efficiencies, the addition of iron oxide magnetic nanoparticles induces the formation of active sites interacting with arsenite.

The post-pyrolysis of magnetic carbon nanocomposites decreases the adsorption of arsenite compared to magnetic carbon nanocomposites obtained by direct co-precipitation method. The carbon coat can contribute to the reduction of As adsorption compared to the magnetic carbon nanocomposites. However, the removal efficiency is higher than for the carbonaceous matrixes.

Acknowledgements Ph.D. student Aura Alejandra Burbano Patiño acknowledges CONICET (Argentina) for her fellowship and Minciencias (Ministerio de Ciencia, Tecnología e Investigación de Colombia). Maria Fernanda Horst and Verónica Leticia Lassalle acknowledge CONICET, UNS, and ANPCyT (Argentina).

Authors contribution All authors whose names appear on the submission: made substantial contributions to the conception and design of the work; the acquisition, analysis, and the interpretation of data. Drafted the work or revised it critically for important intellectual content; approved the version to be published; and agree to be accountable for all aspects of the work in ensuring that questions related to the accuracy or integrity of any part of the work are appropriately investigated and resolved.

Funding Open Access funding provided thanks to the CRUE-CSIC agreement with Springer Nature. This research has been funded by Ministerio de Ciencia, Innovación y Universidades (MCIU), Agencia Estatal de Investigación (AEI), and Fondo Europeo de Desarrollo Regional (FEDER) with grant number RTI2018-096695-B-C31. It also has been funded by Consejo Nacional de Investigaciones Científicas y Tecnológicas (CONICET), Ministerio de Ciencia Tecnología e Innovación (MinCyT) and Universidad Nacional del Sur (Argentina).

Declarations

Conflict of interests The authors declares that there is no conflict of interest to disclose.

References

Ahmaruzzaman M (2022) Magnetic nanocomposite adsorbents for abatement of arsenic species from water and wastewater. Environ Sci Pollut Res 29:82681–82708. https://doi.org/10.1007/s11356-022-23357-2

Alka S, Shahir S, Ibrahim N, Ndejiko MJ, Vo D-VN, Manan FA (2021) Arsenic removal technologies and future trends: a mini review. J Clean Prod 278:123805. https://doi.org/10.1016/j.jclepro.2020.123805

Alkurdi SSA, Al-Juboori RA, Bundschuh J, Bowtell L, Marchuk A (2021) Inorganic arsenic species removal from water using bone char: a detailed study on adsorption kinetic and isotherm models using error functions analysis. J Hazard Mater 405:124112. https://doi.org/10.1016/j.jhazmat.2020.124112

Bali AS, Sidhu GPS (2021) Arsenic acquisition, toxicity and tolerance in plants—from physiology to remediation: a review. Chemosphere 283:131050. https://doi.org/10.1016/j.chemosphere.2021.131050

Bundschuh J, Litter MI, Parvez F, Román-Ross G, Nicolli HB, Jean JS, Liu CW, López D, Armienta MA, Guilherme LRG, Cuevas AG, Cornejo L, Cumbal L, Toujaguez R (2012) One century of arsenic exposure in Latin America: a review of history and occurrence from 14 countries. Sci Total Environ 429:2–35. https://doi.org/10.1016/j.scitotenv.2011.06.024

Burbano AA, Medina GAM, Sánchez FH, Lassalle VL, Horst MF, Gascó G, Méndez A (2022) Influence of post-pyrolysis treatment on physicochemical properties and acid medium stability of magnetic carbon nanocomposites. Biomass Conv Bioref. https://doi.org/10.1007/s13399-022-03517-7

Burbano AA, Gascó G, Horst F, Lassalle V, Méndez A (2023) Production, characteristics, and use of magnetic biochar nanocomposites as sorbents. Biomass Bioenergy 172:106772. https://doi.org/10.1016/j.biombioe.2023.106772

Colomba A, Berruti F, Briens C (2022) Model for the physical activation of biochar to activated carbon. J Anal Appl Pyrolysis 168:105769. https://doi.org/10.1016/j.jaap.2022.105769

European Commission 2023 (2023) Study on the critical raw materials for the EU 2023. Final Report. https://data.europa.eu/doi/https://doi.org/10.2873/725585

Fang Z, Deng Z, Liu A, Zhang X, Lv L, Pan B (2021) Enhanced removal of arsenic from water by using sub-10 nm hydrated zirconium oxides confined inside gel-type anion exchanger. J Hazard Mater 414:125505. https://doi.org/10.1016/j.jhazmat.2021.125505

Fatoki JO, Badmus JA (2022) Arsenic as an environmental and human health antagonist: a review of its toxicity and disease initiation. J Hazard Mater Adv 5:100052. https://doi.org/10.1016/j.hazadv.2022.100052

Habuda-Stanić M, Nujić M (2015) Arsenic removal by nanoparticles: a review. Environ Sci Pollut Res 22:8094–8123. https://doi.org/10.1007/s11356-015-4307-z

Hao L, Liu M, Wang N, Li G (2018) A critical review on arsenic removal from water using iron-based adsorbents. RSC Adv 8:39545. https://doi.org/10.1039/C8RA08512A

Ho YS, McKay G (1999) Pseudo-second order model for sorption processes. Process Biochem 34(5):451–465. https://doi.org/10.1016/S0032-9592(98)00112-5

Horst MF, Alvarez M, Lassalle VL (2016) Removal of heavy metals from wastewater using magnetic nanocomposites: analysis of the experimental conditions. Sep Sci Technol 51(3):550–563. https://doi.org/10.1080/01496395.2015.1086801

Horst MF, Coral DF, Fernández Van Raap MB, Álvarez M, Lassalle V (2017) Hybrid nanomaterials based on gum Arabic and magnetite for hyperthermia treatments. Mater Sci Eng, C 74:443–450. https://doi.org/10.1016/j.msec.2016.12.035

Hsiao C-H, Gupta S, Lee C-Y, Tai N-H (2023) Effects of physical and chemical activations on the performance of biochar applied in supercapacitors. Appl Surf Sci 610:155560. https://doi.org/10.1016/j.apsusc.2022.155560

Kabir F, Chowdhury S (2017) Arsenic removal methods for drinking water in the developing countries: technological developments and research needs. Environ Sci Pollut Res 24:24102–24120. https://doi.org/10.1007/s11356-017-0240-7

Kang K, Nanda S, Hu Y (2022) Current trends in biochar application for catalytic conversion of biomass to biofuels. Catal Today 404:3–18. https://doi.org/10.1016/j.cattod.2022.06.033

Lata S, Samadder SR (2016) Removal of arsenic from water using nano adsorbents and challenges: a review. J Environ Manag 166:387–406. https://doi.org/10.1016/j.jenvman.2015.10.039

Leng L, Xiong Q, Yang L, Li H, Zhou Y, Zhang W, Jiang S, Li H, Huang H (2021) An overview on engineering the surface area and porosity of biochar. Sci Total Environ 763:144204. https://doi.org/10.1016/j.scitotenv.2020.144204

Litter MI, Morgada ME, Bundschuh J (2010) Possible treatments for arsenic removal in Latin American waters for human consumption. Environ Pollut 158(5):1105–1118. https://doi.org/10.1016/j.envpol.2010.01.028

Liu CH, Chuang YH, Chen TY, Tian Y, Li H, Wang MK, Zhang W (2015) Mechanism of arsenic adsorption on magnetite nanoparticles from water: thermodynamic and spectroscopic studies. Environ Sci Technol 49(13):7726–7734. https://doi.org/10.1021/acs.est.5b00381

Low YW, Yee KF (2021) A review on lignocellulosic biomass waste into biochar-derived catalyst: current conversion techniques, sustainable applications and challenges. Biomass Bioenergy 154:106245. https://doi.org/10.1016/j.biombioe.2021.106245

Méndez A, Álvarez ML, Fidalgo JM, Di Stasi C, Manyà JJ, Gascó G (2022) Biomass-derived activated carbon as catalyst in the leaching of metals from a copper sulfide concentrate. Miner Eng 183:107594. https://doi.org/10.1016/j.mineng.2022.107594

Navarathna CM, Karunanayake AG, Gunatilake SR, Pittman CU, Perez F, Mohan D, Mlsna T (2019) Removal of Arsenic (III) from water using magnetite precipitated onto Douglas fir biochar. J Environ Manag 250:109429. https://doi.org/10.1016/j.jenvman.2019.109429

Pezeshki H, Hashemi M, Rajabi S (2023) Removal of arsenic as a potentially toxic element from drinking water by filtration: a mini review of nanofiltration and reverse osmosis techniques. Heliyon 9(3):e14246. https://doi.org/10.1016/j.heliyon.2023.e14246

Qin F, Zhang C, Zeng G, Huang D, Tan X, Abing Duan A (2022) Lignocellulosic biomass carbonization for biochar production and characterization of biochar reactivity. Renew Sustain Energy Rev 157:112056. https://doi.org/10.1016/j.rser.2021.112056

Qiu S, Qiu T, Yan H, Long Q, Wu H, Li X, Zhu D (2022) Investigation of protonation and deprotonation processes of kaolinite and its effect on the adsorption stability of rare earth elements. Colloids Surf A Physicochem Eng Asp 642:128596. https://doi.org/10.1016/j.colsurfa.2022.128596

Qu J, Shi J, Wang Y, Tong H, Zhu Y, Xu L, Wang Y, Zhang B, Tao Y, Dai X, Zhang H, Zhang Y (2022) Applications of functionalized magnetic biochar in environmental remediation: a review. J Hazard Mater 434:128841. https://doi.org/10.1016/j.jhazmat.2022.128841

Rathi BS, Kumar PS (2021) A review on sources, identification and treatment strategies for the removal of toxic arsenic from water system. J Hazard Mater 418:126299. https://doi.org/10.1016/j.jhazmat.2021.126299

Revellame ED, Fortela DL, Sharp W, Hernandez R, Zappi ME (2020) Adsorption kinetic modeling using pseudo-first order

and pseudo-second order rate laws: a review. Clean Eng Technol 1:100032. https://doi.org/10.1016/j.clet.2020.100032

Saravanan A, Yaashikaa PR, Kumar PS, Karishma S, Thamarai P, Deivayanai VC, Rangasamy G, Selvasembian R, Aminabhavi TM (2023) Environmental sustainability of toxic arsenic ions removal from wastewater using electrodeionization. Sep Purif Technol 317:123897. https://doi.org/10.1016/j.seppur.2023.123897

Scheverin VN, Russo A, Grünhut M, Horst MF, Jacobo S, Lassalle VL (2022) Novel iron-based nanocomposites for arsenic removal in groundwater: insights from their synthesis to implementation for real groundwater remediation. Environ Earth Sci 81:188. https://doi.org/10.1007/s12665-022-10286-z

Shahrashoub M, Bakhtiari S (2021) The efficiency of activated carbon/magnetite nanoparticles composites in copper removal: Industrial waste recovery, green synthesis, characterization, and adsorption-desorption studies. Microporous Mesoporous Mater 311:110692. https://doi.org/10.1016/j.micromeso.2020.110692

Song B, Li Q, Cao Q (2024) A mini-review regarding the control techniques available for arsenic contamination from flue gas and water. J Environ Chem Eng 12(2):112249. https://doi.org/10.1016/j.jece.2024.112249

Sri Shalini S, Palanivelu K, Ramachandran A, Raghavan V (2021) Biochar from biomass waste as a renewable carbon material for climate change mitigation in reducing greenhouse gas emissions—a review. Biomass Conv Bioref 11:2247–2267. https://doi.org/10.1007/s13399-020-00604-5

Truong Q-M, Ho P-N-T, Nguyen T-B, Chen W-H, Bui X-T, Patel AK, Singhania RR, Chen C-W, Dong C-D (2022) Magnetic biochar derived from macroalgal Sargassum hemiphyllum for highly efficient adsorption of Cu(II): influencing factors and reusability. Bioresour Technol 361:127732. https://doi.org/10.1016/j.biortech.2022.127732

Uddin MJ, Jeong YK (2020) Review: Efficiently performing periodic elements with modern adsorption technologies for arsenic removal. Environ Sci Pollut Res 27:39888–39912. https://doi.org/10.1007/s11356-020-10323-z

Viraraghavan T, Subramanian KS, Aruldoss JA (1999) Arsenic in drinking water-problems and solutions. Water Sci Technol 40:69–76. https://doi.org/10.1016/S0273-1223(99)00432-1

Wang S, Gao B, Zimmerman AR, Li Y, Ma L, Harris WG, Migliaccio KW (2015) Removal of arsenic by magnetic biochar prepared from pinewood and natural hematite. Bioresour Technol 175:391–395. https://doi.org/10.1016/j.biortech.2014.10.104

WHO (2017) Guidelines for drinking-water quality. 4th Edition, World Health Organization, Geneva, Licence: CC BY-NC-SA 3.0 IGO https://apps.who.int/iris/bitstream/10665/254637/1/9789241549950-eng.pdf

Xu J, Liu Z, Zhao D, Gao N, Fu X (2020) Enhanced adsorption of perfluorooctanoic acid (PFOA) from water by granular activated carbon supported magnetite nanoparticles. Sci Total Environ 723:137757. https://doi.org/10.1016/j.scitotenv.2020.137757

Yihunu EW, Minale M, Abebe S, Limin M (2019) Preparation, characterization and cost analysis of activated biochar and hydrochar derived from agricultural waste: a comparative study. SN Appl Sci 1:873. https://doi.org/10.1007/s42452-019-0936-z

Zama EF, Zhu Y-G, Reid BJ, Sun G-X (2017) The role of biochar properties in influencing the sorption and desorption of Pb(II), Cd(II) and As(III) in aqueous solution. J Clean Prod 148:127–136. https://doi.org/10.1016/j.jclepro.2017.01.125

Zhang S, Li X, Chen JP (2010) An XPS study for mechanisms of arsenate adsorption onto a magnetite-doped activated carbon fiber. J Colloid Interface Sci 343:232–238. https://doi.org/10.1016/j.jcis.2009.11.001

Zhou Y, Qin S, Verma S, Sar T, Sarsaiya S, Ravindran B, Liu T, Sindhu R, Patel AK, Binod P, Varjani S, Singhnia RR, Zhang Z, Awasthi MK (2021) Production and beneficial impact of biochar for environmental application: a comprehensive review. Bioresour Technol 337:125451. https://doi.org/10.1016/j.biortech.2021.125451